J. Fluid Mech. (1969), *vol.* 39, *part* 1, *pp.* 87–96
Printed in Great Britain

Fluid line growth in grid-generated isotropic turbulence

By S. CORRSIN AND M. KARWEIT†
Mechanics Department, The Johns Hopkins University

(Received 26 February 1969)

Fluid material line growth in turbulent flow has been measured by tagging lines with small hydrogen bubbles in the nearly isotropic turbulence behind a regular grid in a water tunnel. The average three-dimensional line lengths were inferred by an intersection-counting method carried out on one-plane photographs. The measurements cover 'small' time intervals only.

Introduction

The importance of fluid material line growth in turbulent flow was emphasized first by Taylor (1938) in connexion with vorticity production by the growth of vortex lines. Vortex lines are approximately‡ fluid lines, in high Reynolds number flows. Specifically, in high Reynolds number turbulence the larger scale behaviour of vortex lines is presumably that of fluid lines while geometrical traits of the order of the Kolmogorov microscale and smaller are strongly affected by viscous diffusion and destruction of vorticity.

There is no reason to expect that the material lines which coincide with vortex lines grow at a rate typical of all material lines. In fact the work of Reid cited below gives a definite difference in the growth fluctuations.

The general question of fluid material line growth in isotropic turbulence was taken up theoretically by Batchelor (1952), who offered the plausible conjecture that asymptotically (for large enough time) in stationary homogeneous turbulence the number of eddies of each size acting to stretch a long fluid material line is just proportional to its length. This has as immediate consequence an exponentially growing mean line length.

Apparently the only other paper directly on the subject is also a theoretical one, by Reid (1955). Following Batchelor, he estimated the growth in isotropic turbulence of a passive solenoidal axial vector field **F** whose field lines are fluid material lines. This last property excludes molecular diffusion, and can alternatively be described by saying that the field 'flux' through any segment of fluid material area is independent of time. To make the moment problem determinate, Reid postulated that fourth moments could be expressed in terms of second moments as though the variables were jointly normal. This provided an estimate of the mean square value of line element length, $\overline{\delta^2}(t)$. But this does not include the information appropriate for estimating the average length

† Also: Chesapeake Bay Institute. ‡ I.e. for a limited time.

$\overline{\delta}(t)$, and our experiments provide no data on $\overline{\delta^2}$, so we pursue Reid's analysis no further.

This paper presents some measurements of mean line length for small times after marking, and offers as check a 'small t' analysis which permits the use of independently measured Eulerian frame properties.

The experiment

Approximate tagging of a fluid material line was achieved with the 'hydrogen bubble' electrolysis method (Geller 1954; Clutter & Smith 1961; Schraub, *et al.* 1964; Mattingly 1966; Karweit 1968). A 0·001 in. platinum wire was stretched normal to the mean flow in a water tunnel, 18 mesh lengths behind a square-mesh round-rod turbulence generating grid. The grid solidity was 0·34, to match that used by Batchelor & Townsend (1948), because the Reynolds number in this experiment is closer to their low values than to that of other published experiments. The mesh size is $M = \frac{1}{2}$ in. and the mean speed is 4·0 in./sec, giving a grid Reynolds number $R_M \equiv \overline{U}M/\nu = 1360$, where ν is kinematic viscosity. The rods were $\frac{3}{32}$ in. in diameter.

The water tunnel was made some years ago by Sparks & Hoelscher (1962).† It has an 8 in. square test section 48 in. in length. This length limitation prevented placing the tagging wire a more suitable distance (farther) from the grid (the turbulence may have detectable lateral inhomogeneity to $x/M = 30$ or 40 (Corrsin 1963)). x is distance from the grid.

The free stream (empty tunnel) mean velocity field was slightly non-uniform, but the effect on line growth was within the uncertainty of the experiment.

Figure 1 (plate 1) is a typical photograph from which fluid material line length was measured. Double lines had been generated to permit the study of relative dispersion, but that is another story. For material line growth, only the thinner member of each pair was analyzed.

The analysis was carried out according to an equation relating the length of a three-dimensional, stationary, random, multiple-valued function to the number of cuts experienced by sampling planes making all angles with the axis (Corrsin & Phillips 1961, especially §6). For a function which is statistically axisymmetric the relevant equation is

$$\overline{\Lambda} = 2\int_0^{\frac{1}{2}\pi} \mu(\gamma) \cos\gamma \sin\gamma \, d\gamma, \tag{1}$$

where $\overline{\Lambda}$ is the average contour length per unit axis length, thus the ratio of fluid material line length to initial length. γ is the angle between the normal to any 'sampling' plane and the axis (the initial fluid material line configuration). $\mu(\gamma)$ is the average number of intersections between the random contour and all sampling planes at angle γ. With a collection of plane photographs like figure 1, $\mu(\gamma)$ is obtained for a downstream distance x by simply drawing a series of straight lines at angle $(\frac{1}{2}\pi - \gamma)$ to the axis (which is normal to the mean flow), counting intersections and averaging over enough cases to give reasonably small scatter.

† See also Karweit (1968).

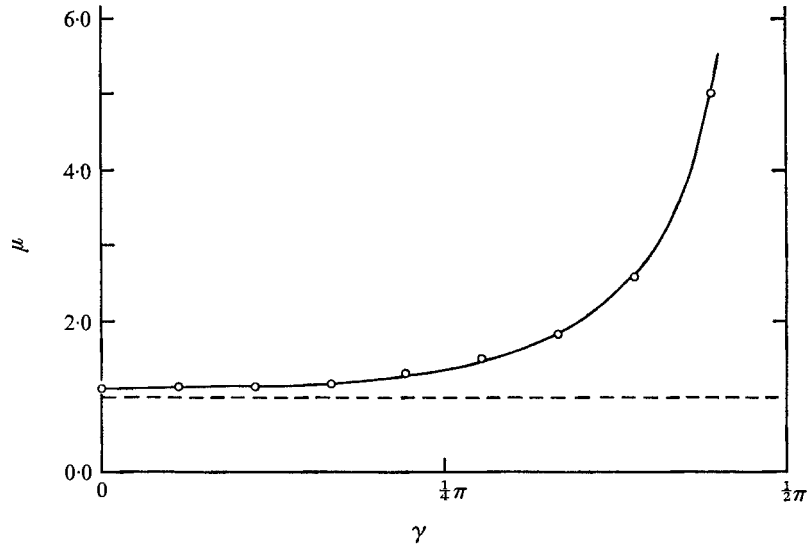

FIGURE 2. A typical measurement of average number of intersections of a bubble line photograph as a function of γ, the angle between sampling line and bubble line axis. Note that it is slightly multiple-valued [$\gamma(0) > 1{\cdot}0$].

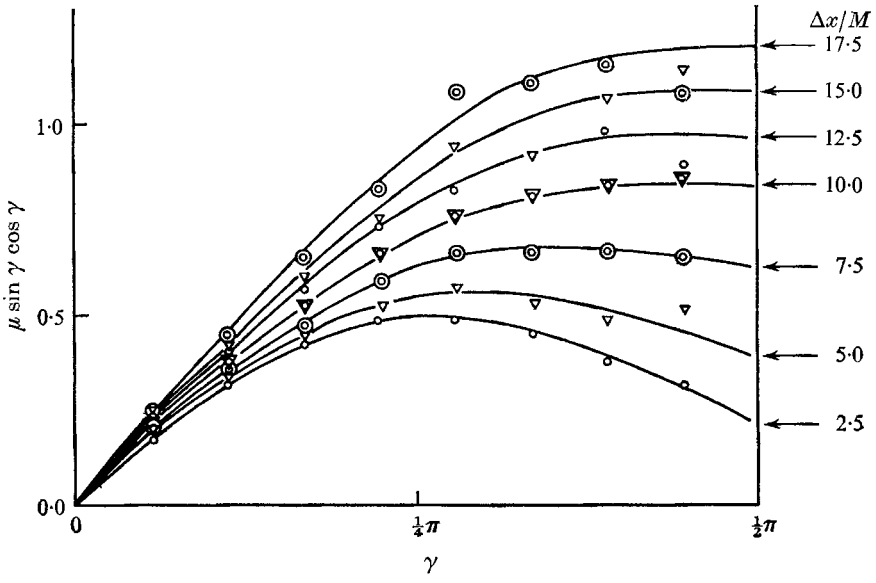

FIGURE 3. The integrand of equation (1) at seven downstream distances. Curve fairing was done on a 'family' basis.

Figure 2 shows a typical measurement of $\mu(\gamma)$, the case $(x-x_0)/M = 10$. $x_0/M = 18$ is the position of the tagging wire. $\mu(\gamma)$ must go to infinity for $\gamma = \frac{1}{2}\pi$, and it is inconvenient to measure for $\gamma \geqslant 80°$. Furthermore, extrapolation is an uncertain business around singularities. Therefore, the extrapolation to $\gamma = \frac{1}{2}\pi$ was done for the product $\mu(\gamma)\cos\gamma\sin\gamma$, figure 3. We have not yet established a general theoretical value for this product at the boundary $\gamma = \frac{1}{2}\pi$. In the simple case of a helical (single valued) contour it can be shown that the asymptotic behaviour is

$$\mu(\gamma)\cos\gamma\sin\gamma \to 4R/P + (\tfrac{1}{2}\pi - \gamma). \tag{2}$$

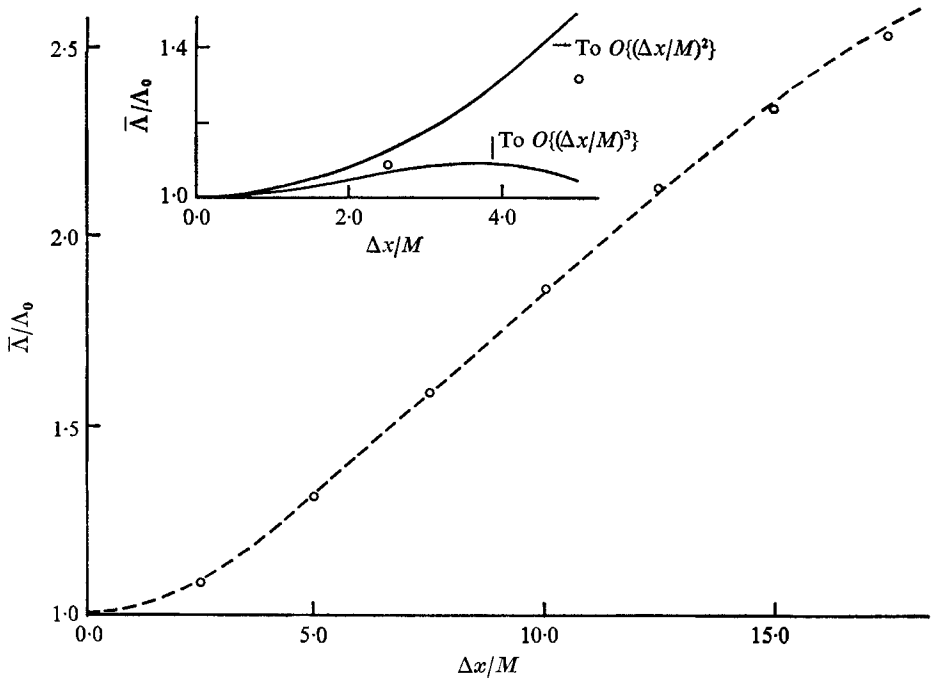

FIGURE 4. Average fluid line length as a function of distance from tagging location ($x/M = 18$ behind grid). The solid curve is a truncated power series evaluated to the cubic term by independent measurements (equation (27)). – – –, empirical curve from 'Lagrangian' data points. ——, empirical 'small time' curves estimated from 'Eulerian data'.

In this special case the integrand has a maximum at $\gamma \leqslant \frac{1}{2}\pi$. R is the radius of the helix, P is its wavelength (pitch). Figure 3 shows that $\mu(\gamma)\cos\gamma\sin\gamma$ also has a maximum at $\gamma < \frac{1}{2}\pi$ for the experimental multiple-valued cases.

The experimental result for relative mean fluid material line length as a function of dimensionless time is plotted in figure 4.

Eulerian estimate for small times

In order to check the accuracy of part of the experimental results, we can estimate the fluid line growth in terms of more commonly available (Eulerian or spatial frame) statistical properties of the turbulence. The comparison to be

shown is useful only for 'small time'. Terms with higher powers of t include higher-order Eulerian moments, for which we have no data.

In a material ('Lagrangian') frame the position $\mathbf{X}$ of a fluid point can be considered as a function of time t and of its position $\mathbf{X}_0$ at a reference time $t = 0$:

$$\mathbf{X} = \mathbf{X}(\mathbf{X}_0, t), \tag{3}$$

where

$$\mathbf{X}_0 \equiv \mathbf{X}(\mathbf{X}_0, 0).$$

A material differential line element can be identified at time t by

$$d\boldsymbol{\Lambda} = \mathbf{X}(\mathbf{X}_0 + d\mathbf{X}_0, t) - \mathbf{X}(\mathbf{X}_0, t). \tag{4}$$

Expanding the first term on the right in series about $\mathbf{X}_0$, and truncating properly for infinitesimal $d\mathbf{X}_0 \equiv d\boldsymbol{\Lambda}_0$, we have

$$d\Lambda_i = \frac{\partial X_i}{\partial X_{0_j}} d\Lambda_{0_j}, \tag{5}$$

where Cartesian co-ordinates are used for convenience.

The length of a finite line is the line integral of the magnitudes

$$(d\Lambda_i d\Lambda_i)^{\frac{1}{2}} = \left(\frac{\partial X_k}{\partial X_{0_j}} \frac{\partial X_k}{\partial X_{0_m}} d\Lambda_{0_j} d\Lambda_{0_m}\right)^{\frac{1}{2}}. \tag{6}$$

The expression of $\Lambda(t) \equiv |\boldsymbol{\Lambda}(t)|$ as a line integral with element $d\boldsymbol{\Lambda}_0 = d\mathbf{X}_0$ is simplest when the initial configuration is a straight line along a single Cartesian axis direction:

$$\Lambda(t) = \int_0^{\Lambda_0} \left\{\left(\frac{\partial X_1}{\partial X_{0_2}}\right)^2 + \left(\frac{\partial X_2}{\partial X_{0_2}}\right)^2 + \left(\frac{\partial X_3}{\partial X_{0_2}}\right)\right\}^{\frac{1}{2}} dX_{0_2}. \tag{7}$$

This corresponds to the experimental arrangement, $d\Lambda_{0_1} = d\Lambda_{0_3} = 0$.

The average length can be written as the integral of an averaged function when the method of averaging commutes with the integration operation. The ensemble average is an example, and we assume for simplicity that it is used:

$$\overline{\Lambda}(t) = \int_0^{\Lambda_0} \overline{\left(\frac{\partial X_i}{\partial X_{0_2}} \frac{\partial X_i}{\partial X_{0_2}}\right)^{\frac{1}{2}}} dX_{0_2}. \tag{8}$$

But we restrict to homogeneous turbulence, so all line elements undergo the same statistical history, and the average is independent of the integration. Therefore

$$\overline{\Lambda}(t) = \Lambda_0 \overline{\left(\frac{\partial X_i}{\partial X_{0_2}} \frac{\partial X_i}{\partial X_{0_2}}\right)^{\frac{1}{2}}}. \tag{9}$$

The experimental procedure is a combination of an ensemble average (photographs taken at different times, some of them hours apart) and a spatial average equally weighted along the x_2-axis.

For the limiting case of 'very small time' we can approximate the right side of (9) in terms of Eulerian frame statistical properties of the turbulence. These properties are ordinarily more accessible to both theory (because of the simpler

form of the Navier–Stokes equations) and experiment (because of the usefulness of the hot-wire anemometer).

In general,

$$X_i(\mathbf{X}_0, t) = X_{0_i} + \int_0^t V_i(\mathbf{X}_0, t')\, dt' \tag{10}$$

and

$$\frac{\partial X_i}{\partial X_{0_k}} = \delta_{ik} + \int_0^t \frac{\partial V_i}{\partial X_{0_k}} dt'. \tag{11}$$

δ_{ik} is the 'Kronecker delta', equal to 1 when $i = k$, zero otherwise. With $\mathbf{V}(\mathbf{X}_0, t)$ expanded in time series about $t = 0$,

$$\frac{\partial V_i}{\partial X_{0_k}}(\mathbf{X}_0, t) = \frac{\partial V_i}{\partial X_{0_k}}(\mathbf{X}_0, 0) + \frac{\partial^2 V_i}{\partial t\, \partial X_{0_k}}(\mathbf{X}_0, 0)t + \frac{\partial^3 V_i}{\partial^2 t\, \partial X_{0_k}}(\mathbf{X}_0, 0)\frac{t^2}{2!} + \ldots. \tag{12}$$

But these Lagrangian spatial derivatives at $t = 0$ are the same as Eulerian spatial derivatives because $\mathbf{X}_0$ is defined as the value of $\mathbf{X}$ at $t = 0$. The Lagrangian $\partial/\partial t$ is the same as the Eulerian 'Stokes derivative'. Equation (12) can therefore be written as

$$\frac{\partial V_i}{\partial X_{0_k}} = \left\{\frac{\partial u_i}{\partial x_k}\right\}_{t=0} + \left\{\left(\frac{\partial}{\partial t} + u_j \frac{\partial}{\partial x_j}\right)\frac{\partial u_i}{\partial x_k}\right\}_{t=0} t + \left\{\left(\frac{\partial}{\partial t} + u_m \frac{\partial}{\partial x_m}\right)\left(\frac{\partial}{\partial t} + u_j \frac{\partial}{\partial x_j}\right)\frac{\partial u_i}{\partial x_k}\right\}_{t=0} \frac{t^2}{2!} + \ldots. \tag{13}$$

Substituting this into (11), integrating term-by-term, and squaring, we get terms inside the square root of (9) like

$$\left(\frac{\partial X_1}{\partial X_{0_2}}\right)^2 = \int_0^t \int_0^t \left\{\left(\frac{\partial u_1}{\partial x_2}\right)^2_{t=0} + \left(\frac{\partial u_1}{\partial x_2}\right)_{t=0}\left(\frac{\partial^2 u_1}{\partial t\, \partial x_2} + u_j \frac{\partial^2 u_1}{\partial x_j \partial x_2}\right)_{t=0} t' + \left(\frac{\partial u_1}{\partial x_2}\right)_{t=0}\left(\frac{\partial^2 u_1}{\partial t\, \partial x_2} + u_j \frac{\partial^2 u_1}{\partial x_j \partial x_2}\right)_{t=0} t'' + \ldots\right\} dt'\, dt''.$$

Therefore

$$\left(\frac{\partial X_1}{\partial X_{0_2}}\right)^2 = \left(\frac{\partial u_1}{\partial x_2}\right)^2_{t=0} t^2 + \left(\frac{\partial u_1}{\partial x_2}\right)_{t=0}\left(\frac{\partial^2 u_1}{\partial t\, \partial x_2} + u_j \frac{\partial^2 u_1}{\partial x_j \partial x_2}\right)_{t=0} t^3 + \ldots. \tag{14}$$

Also

$$\left(\frac{\partial X_2}{\partial X_{0_2}}\right)^2 = 1 + 2\int_0^t \left\{\left(\frac{\partial u_2}{\partial x_2}\right)_{t=0} + \left(\frac{\partial^2 u_2}{\partial t\, \partial x_2} + u_j \frac{\partial^2 u_2}{\partial x_j \partial x_2}\right)_{t=0} t' + \left[\left(\frac{\partial}{\partial t} + u_i \frac{\partial}{\partial x_i}\right)\left(\frac{\partial^2 u_2}{\partial t\, \partial x_2} + u_j \frac{\partial^2 u_2}{\partial x_j \partial x_2}\right)\right]_{t=0} \frac{t'^2}{2} + \ldots\right\} dt'$$
$$+ \int_0^t \int_0^t \left\{\left(\frac{\partial u_2}{\partial x_2}\right)^2_{t=0} + \left(\frac{\partial u_2}{\partial x_2}\right)_{t=0}\left(\frac{\partial^2 u_2}{\partial t\, \partial x_2} + u_j \frac{\partial^2 u_2}{\partial x_j \partial x_2}\right)_{t=0} t' + \left(\frac{\partial u_2}{\partial x_2}\right)_{t=0}\left(\frac{\partial^2 u_2}{\partial t\, \partial x_2} + u_j \frac{\partial^2 u_2}{\partial x_j \partial x_2}\right)_{t=0} t'' + \ldots\right\} dt'\, dt'',$$

therefore

$$\left(\frac{\partial X_2}{\partial X_{0_2}}\right)^2 = 1 + 2\left(\frac{\partial u_2}{\partial x_2}\right)_{t=0} t + \left[\left(\frac{\partial u_2}{\partial x_2}\right)^2 + \frac{\partial^2 u_2}{\partial t\,\partial x_2} + u_j \frac{\partial^2 u_2}{\partial x_j \partial x_2}\right]_{t=0} t^2$$
$$+ \left[\frac{\partial u_2}{\partial x_2}\frac{\partial^2 u_2}{\partial t\,\partial x_2} + u_j \frac{\partial u_2}{\partial x_2}\frac{\partial^2 u_2}{\partial x_j \partial x_2} + \frac{1}{3}\frac{\partial^3 u_2}{\partial t^2 \partial x_2} + \frac{1}{3}\frac{\partial^2}{\partial x_i \partial t}\left(u_i \frac{\partial u_2}{\partial x_2}\right)\right.$$
$$\left. + \frac{1}{3}\frac{\partial}{\partial x_k}\left(u_k \frac{\partial^2 u_2}{\partial t\,\partial x_2}\right) + \frac{1}{3}\frac{\partial}{\partial x_i}\left(u_i u_k \frac{\partial^2 u_2}{\partial x_k \partial x_2}\right)\right]_{t=0} t^3 + \ldots. \tag{15}$$

$(\partial X_3/\partial X_{0_2})^2$ is the same as (14), but with u_3 in place of u_1.

Next we substitute (14) and (15) into (9), expand the square root by the binomial expansion, neglect all terms with powers of t higher than the third, and average. Further, we restrict to exactly isotropic turbulence, which must be homogeneous and decay with increasing time. The result is

$$\frac{\overline{\Lambda}(t)}{\Lambda_0} \approx 1 + \overline{\left(\frac{\partial u_1}{\partial x_2}\right)^2}_{t=0} t^2 + \left[\frac{1}{2}\frac{d}{dt}\overline{\left(\frac{\partial u_1}{\partial x_2}\right)^2} - \overline{\frac{\partial u_2}{\partial x_2}\left(\frac{\partial u_1}{\partial x_2}\right)^2}\right]_{t=0} t^3. \tag{16}$$

Experimental results related to these Eulerian moments in wind-tunnel turbulence behind a similar grid at comparable Reynolds numbers are given by Batchelor & Townsend (1948). The second moments can be expressed in terms of velocity moments and the 'Taylor microscale', the abcissa-intercept of the Kármán–Howarth 'g-type' correlation function (see, for example, Hinze 1959, especially chapter 1):

$$\overline{\left(\frac{\partial u_1}{\partial x_2}\right)^2} = 2\frac{\overline{u_1^2}}{\lambda^2}. \tag{17}$$

The first part of the t^3 coefficient can be expressed in the same variables if we use Taylor's energy decay equation

$$\frac{d\overline{u_1^2}}{dt} = -10\nu\frac{\overline{u_1^2}}{\lambda^2}. \tag{18}$$

Then

$$\frac{d}{dt}\overline{\left(\frac{\partial u_1}{\partial x_2}\right)^2} = 2\frac{d}{dt}\left(\frac{\overline{u_1^2}}{\lambda^2}\right) \approx -40\nu\frac{\overline{u_1^2}}{\lambda^4}. \tag{19}$$

The last step in this chain is a consequence of their observation that $(\overline{u_1^2}\lambda^2)$ was nearly constant during an 'initial period' extending over perhaps

$$20M < x < 100M.$$

The third-order moment in (16) can be expressed in terms of a Kármán–Howarth triple correlation function. A simple demonstration starts with the equality

$$\overline{\left(\frac{\partial u_2}{\partial x_2}\right)\left(\frac{\partial u_1}{\partial x_2}\right)^2} = \frac{\partial}{\partial x_2}\overline{\left[u_2\left(\frac{\partial u_1}{\partial x_2}\right)^2\right]} - 2\overline{u_2\frac{\partial u_1}{\partial x_2}\frac{\partial^2 u_1}{\partial x_2^2}}.$$

Then the first term is dropped by homogeneity. By inspection of the series expansion of the $h(r)$ triple correlation function

$$\overline{u_2\frac{\partial u_1}{\partial x_2}\frac{\partial^2 u_1}{\partial x_2^2}} = -\frac{\overline{u_1^2}^{\frac{3}{2}}}{6}h'''(0) - \tfrac{1}{6}\overline{u_1 u_2\frac{\partial^3 u_1}{\partial x_2^3}},$$

and by expansion of the $q(r)$ triple correlation function,

$$\overline{u_1 u_2 \frac{\partial^3 u_1}{\partial x_2^3}} = \overline{u_1^2}^{\frac{3}{2}} q'''(0). \tag{20}$$

$h(r)$ and $q(r)$ can each be expressed in terms of the other or in terms of the more conveniently measured function $k(r)$, in which all components are in the same direction. There results

$$\overline{\frac{\partial u_2}{\partial x_2}\left(\frac{\partial u_1}{\partial x_2}\right)^2} = \frac{\overline{u_1^2}^{\frac{3}{2}}}{4} k'''(0) = \overline{\frac{1}{4}\left(\frac{\partial u_1}{\partial x_1}\right)^3},$$

an oft-measured moment. For a wide range of Reynolds numbers, it is found empirically that

$$-\overline{\left(\frac{\partial u_1}{\partial x_1}\right)^3} \doteq 0{\cdot}4 \overline{\left(\frac{\partial u_1}{\partial x_1}\right)^2}^{\frac{3}{2}} = 0{\cdot}4 \frac{\overline{u_1^2}^{\frac{3}{2}}}{\lambda^3}. \tag{21}$$†

The estimate for average line length in terms of easily measured Eulerian quantities is finally

$$\frac{\overline{\Lambda}(t)}{\Lambda_0} \approx 1 + 2\frac{\overline{u_1^2}}{\lambda^2} t^2 + \left[-20\nu \frac{\overline{u_1^2}}{\lambda^4} + \frac{1}{10} \frac{\overline{u_1^2}^{\frac{3}{2}}}{\lambda^3} \right] t^3, \tag{22}$$

with $\overline{u^2}$ and λ evaluated at $t = 0$.

This 'small time' estimate is used to check the results inferred from the hydrogen bubble photographs in the following way: the mean square turbulent velocity components along and across the mean flow direction were measured by exploiting the expression from Taylor's (1921) theory of 'diffusion by continuous movements.',

$$X_i(0,t) \xrightarrow{t \to 0} V_i(0,t)\, t, \tag{23}$$

whence, for example,

$$\overline{u_1^2} = \lim_{t \to 0} \left\{ \frac{\overline{X_1^2}}{t^2} \right\}. \tag{24}$$

$\overline{X}_1^2$ and $\overline{X}_2^2$ were measured from the hydrogen-bubble line displacements, and (24) used to get $\overline{u_1^2} = 0{\cdot}046$ cm^2/sec^2 and $\overline{u_2^2} = 0{\cdot}037$ cm^2/sec^2. From axial symmetry of the experiment we assume $\overline{u_3^2} = \overline{u_2^2}$. Since we are actually estimating velocity derivative statistics [such as $(\overline{\partial u_1/\partial x_2)^2}$], the expectation of some degree of local isotropy in the corresponding fine structure suggests that we use the estimate $\frac{1}{3}\overline{u_k u_k}$ in place of $\overline{u_1^2}$: thus,

$$\overline{\left(\frac{\partial u_1}{\partial x_2}\right)^2} \approx \frac{2}{\lambda^2} [\tfrac{1}{3}(\overline{u_1^2} + \overline{u_2^2} + \overline{u_3^2})]$$

in place of (17), which is valid for exactly isotropic turbulence. Similarly, $\frac{1}{3}\overline{u_k u_k}$ was used in place of $\overline{u_1^2}$ in the t^3 term.

Having no data on λ from this experiment, we turn to the Batchelor–Townsend (1948) data behind a similar grid. One of their least-scattered cases at low

† Batchelor & Townsend (1947); Stewart (1951); Mills *et al.* (1958).

Reynolds number, $R_M = 5500$, gives a (slightly extrapolated) microscale value of $\lambda = 0{\cdot}10$ cm at $x/M = 18$, $M = 1{\cdot}27$ cm. Since our grid Reynolds number is 1360, this λ value must be rescaled. It is generally found that integral scale L is insensitive to grid Reynolds number differences. A principal Reynolds number effect is in the ratio of microscale to integral scale, a ratio for which we can use a Kármán–Howarth (1938) estimate (see also Batchelor (1953) or Hinze (1959)):

$$\frac{\lambda}{L} \sim \frac{1}{R_\lambda} \sim \frac{1}{\sqrt{R_L}}. \tag{25}\dagger$$

$R_\lambda \equiv \sqrt{(\overline{u_1^2})}\lambda/\nu$ and $R_L \equiv \sqrt{(\overline{u_1^2})}L/\nu$. Since L/M and $\overline{u_1^2}/\overline{U}^2$ are insensitive to changes in the various Reynolds numbers,

$$\frac{\lambda}{L} \sim \frac{1}{\sqrt{R_M}}. \tag{26}$$

This relation is more likely to be accurate for turbulence at Reynolds numbers considerably larger than that in this experiment, but no better estimate is available. Application of (26) gives $\lambda \approx 0{\cdot}23$ cm for the present case.

As proposed originally by Taylor, we compare the time variation of theoretical isotropic turbulence with the distance variation of stationary inhomogeneous nearly isotropic turbulence. The correspondence is $\Delta x \leftrightarrow \overline{U}t$ for mean properties. The equation (22) with coefficients determined from hot-wire measurements of Eulerian quantities, as described above, becomes

$$\frac{\overline{\Lambda}(t)}{\Lambda_0} \approx 1 + 0{\cdot}0194\left(\frac{\Delta x}{M}\right)^2 - 0{\cdot}0035\left(\frac{\Delta x}{M}\right)^3. \tag{27}$$

This provides the two curves in the small inset part of figure 4. The points are values measured by the (essentially Lagrangian) line-tagging and intersection-counting method. Unfortunately the Eulerian moments required for the coefficient of the $(\Delta x)^4$ term which extends (27) have not been measured.

Inference of line growth in stationary turbulence

The experimental results for $\overline{\Lambda}(t)$ in figure 4 show no clear approach toward the asymptotic exponential growth anticipated by Batchelor. One obvious reason is that the total elapsed time (about 1·6 sec) from tagging to the last measuring station may be scarcely larger than the basic Eulerian integral time scale T_E which would be observed when travelling with the mean speed. There is some evidence that $T_E = O(L_f/\sqrt{(\overline{u_1^2})})$, where L_f is the integral length scale of the Kármán–Howarth $f(r)$ correlation function (Comte-Bellot & Corrsin, in preparation). For the present experiment this would give $T_E = O$ (1·9 sec).

A second reason may be that the turbulence is decaying. Its characteristic velocity is decreasing while its characteristic scales are all growing. In fact, the

† Although this is a 'large Reynolds number' estimate, it turns out to give fairly good agreement with experiment at moderate Reynolds numbers as well.

decay-term in the coefficient of t^3, (16) or (22), is much larger than the third-moment term. Therefore a crude 'correction' for the effect of decay on the measured $\overline{\Lambda}(t)$ was tried.

The simplest time rescaling is that proposed by Townsend (1951): a new time τ is defined by

$$d\tau = \frac{\sqrt{[\overline{u_1^2}(t)]}}{L(t)} dt.$$

The 'corrected' curve, $\overline{\Lambda}/L$ *vs.* τ, shows no great change in character from $\overline{\Lambda}$ *vs.* τ, so it is not presented here.

This work was supported by the Fluid Dynamics Branch, U.S. Office of Naval Research, and was presented at the Annual Meeting of the Division of Fluid Dynamics, American Physical Society, Seattle, November 1968. We should like to thank James Newton for his work in extracting data from the photographs, and to acknowledge the encouragement of the Society for Statistical Geometry.

REFERENCES

BATCHELOR, G. K. 1952 *Proc. Roy. Soc.* A **213**, 349. [Correction in *Proc. Camb. Phil. Soc.* **51**, 361 (1955).]

BATCHELOR, G. K. 1953 *The Theory of Homogeneous Turbulence*. Cambridge University Press.

BATCHELOR, G. K. & TOWNSEND, A. A. 1947 *Proc. Roy. Soc.* A **190**, 534.

BATCHELOR, G. K. & TOWNSEND, A. A. 1948 *Proc. Roy. Soc.* A **193**, 539.

CLUTTER, D. W. & SMITH, A. M. O. 1961 *Aerosp. Engng.* **20**, 24.

CORRSIN, S. 1963 In *Handbuch der Physik*, VIII/2, ed. by S. Flügge & C. Truesdell. Berlin: Springer-Verlag.

CORRSIN, S. & PHILLIPS, O. M. 1961 *J. Soc. Indust. Appl. Math.* **9**, 395.

GELLER, E. W. 1954 M.S. degree, Mississippi State College.

HINZE, J. O. 1959 *Turbulence*. New York: McGraw-Hill.

KÁRMÁN, T. VON & HOWARTH, L. 1938 *Proc. Roy. Soc.* A **164**, 516.

KARWEIT, M. 1968 M.S.E. degree, Johns Hopkins University.

MATTINGLY, G. E. 1966 *Rep.* 2146, *Hydromech. Div., David Taylor Model Basin.*

MILLS, R. R., KISTLER, A. L., O'BRIEN, V. & CORRSIN, S. 1958 *Nat. Adv. Comm. for Aero. Tech. Note* 4288.

REID, W. H. 1955 *Proc. Camb. Phil. Soc.* **51**, 350.

SCHRAUB, F. A., KLINE, S. J., HENRY, J., RUNSTADLER, P. W. & LITTELL, A. 1964 *Rep.* MD-10, *Mech. Engng. Dept. Stanford University.*

SPARKS, R. & HOELSCHER, H. E. 1692 *A.I.Ch.E. J.* **8**, 103.

STEWART, R. W. 1951 *Proc. Camb. Phil. Soc.* **47**, 146.

TAYLOR, G. I. 1938 *Proc. Roy. Soc.* A **164**, 15.

TOWNSEND, A. A. 1951 *Proc. Roy. Soc.* A **224**, 487.

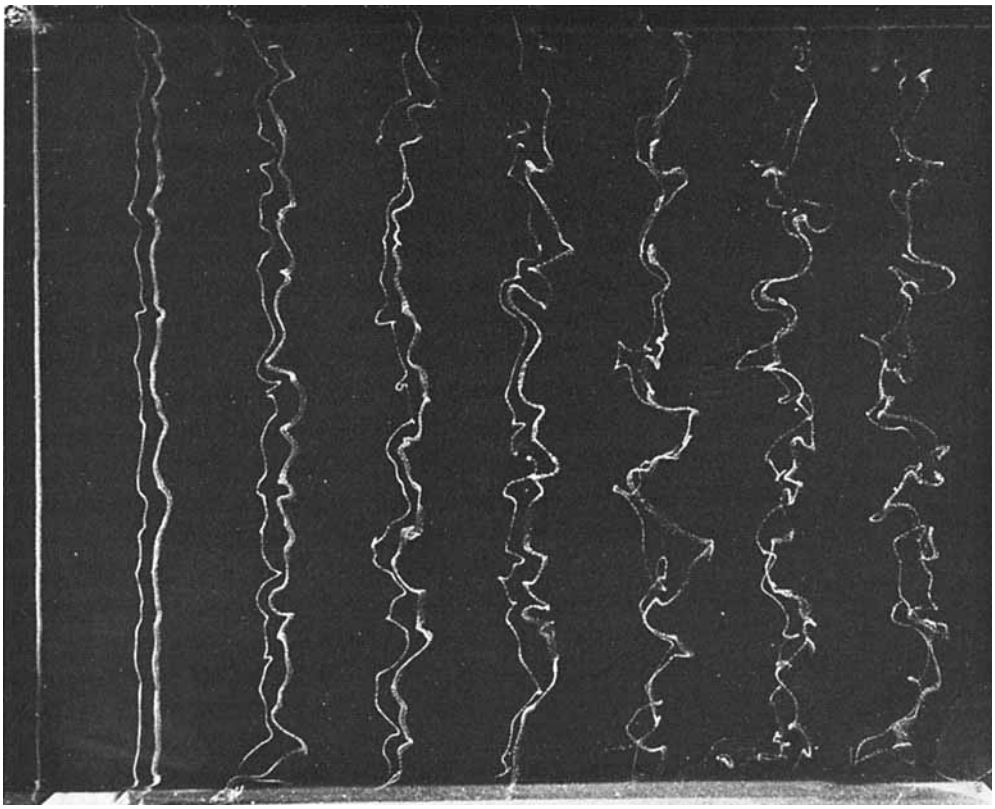

FIGURE 1. A typical photograph of growing lines of hydrogen bubbles initially normal to the flow 18 mesh lengths behind the grid. The wire voltage is pulsed.